JOURNAL OF THERMOPHYSICS AND HEAT TRANSFER
Vol. 12, No. 4, October–December 1998

Heat Transfer Analysis of a Plug-Type Heat Flux Gauge

S. Rooke*
CSO Engineers, Indianapolis, Indiana 46240
and
G. Fralick† and C. Liebert‡
NASA Lewis Research Center, Cleveland, Ohio 44135

An analysis of a miniature plug-type heat flux gauge is presented. The analysis provides previously unavailable quantitative details of the heat transfer within this gauge type. The analysis is performed using a two-dimensional, axisymmetric numerical model with temperature-dependent thermal properties. The model is solved using the alternating direction implicit finite difference solution procedure. Details of the comparison of the model results with experimental data are presented. Isotherms, gauge centerline temperature distributions, and heat fluxes computed at various locations within the gauge are presented and discussed. For the cases studied, the numerical analysis reveals that the measured heat flux indicated by the gauge is not the same as the heat flux at the gauge hot active surface. Using temperatures measured by the gauge as input, the numerical model enables one to compute the heat flux into the surface in which the gauge is mounted, at positions that are thermally undisturbed by the presence of the gauge. This can be done regardless of whether or not the heat flux at the gauge hot active surface is the same as the heat flux into thermally undisturbed portions of the surface.

Nomenclature

A_r = $-CE$, Eq. (3)
A_x = $-CS$, Eq. (2)
B_r = $-CW$, Eq. (3)
B_x = $-CN$, Eq. (2)
CE = $(k_{i,j+1} \times \alpha_{i,j})/(k_{i,j+1} + k_{i,j}) \times (r_{i,j} + 1/2\Delta r)/r_{i,j} \times \Delta t/\Delta r^2$, dimensionless
CN = $(k_{i-1,j} \times \alpha_{i,j})/(k_{i-1,j} + k_{i,j} \times \Delta x_{i-1}/\Delta x_i) \times \Delta t/\Delta x_i^2$, dimensionless
C_r = $CN \times T_{i-1,j}^{n+1/2} + (1 - CN - CS) \times T_{i,j}^{n+1/2} + CS \times T_{i+1,j}^{n+1/2}$, Eq. (3)
CS = $(k_{i+1,j} \times \alpha_{i,j})/(k_{i+1,j} + k_{i,j} \times \Delta x_{i+1}/\Delta x_i) \times \Delta t/\Delta x_i^2$, dimensionless
CW = $(k_{i,j-1} \times \alpha_{i,j})/(k_{i,j-1} + k_{i,j}) \times (r_{i,j} - 1/2\Delta r)/r_{i,j} \times \Delta t/\Delta r^2$, dimensionless
C_x = $CW \times T_{i,j-1}^{n} + (1 - CW - CE) \times T_{i,j}^{n} + CE \times T_{i,j+1}^{n}$, Eq. (2)
D_r = $1 + CW + CE$, Eq. (3)
D_x = $1 + CS + CN$, Eq. (2)
h = convective coefficient, W/m^2 K
k = thermal conductivity, W/m K
q = heat transfer rate, W
q'' = heat flux, W/m^2
$R''_{t,c}$ = interface thermal resistance, m^2 K/W
r = radial position, m
T = temperature, K
t = time, s
x = axial position, m
α = thermal diffusivity, m^2/s
Δr = radial direction node spacing, m
Δt = time increment, s
Δx = axial direction node spacing, m
ε = emissivity

Subscripts
ann = probe stem annular surface
g = gauge
i = axial grid location indicator
j = radial grid location indicator
jet = probe stem jet impingement surface
post, TC = in gauge post, at axial position of thermocouple number that is given
surf, CL = gauge surface, at centerline
surf, p = gauge surface, averaged over post radius
surf, g = gauge surface, averaged over gauge radius
w = wall surface

Superscript
n = time index

Introduction

NUMEROUS heat flux gauge concepts have been studied and a variety of heat flux measurement devices are available. An overview of heat flux measurement techniques is given by Diller.[1] Generally, each heat flux measurement concept has advantages and disadvantages, but the merits of a heat flux measurement device must ultimately be evaluated with careful consideration given to the intended application. The plug-type heat flux gauge has particular merit in applications that require a small sensing element, nonintrusiveness in the flow, and the ability to withstand high temperatures and harsh flow conditions. This gauge type has been shown to give good agreement (±10–20%) with other types of gauges when subjected to heat fluxes up to 10 MW/m^2 (Ref. 2), and has been demonstrated under Space Shuttle main engine turbopump conditions[3] and under high-enthalpy supersonic flow conditions.[4]

A cross-sectional view of a plug-type gauge/probe assembly mounted in a planar wall is shown in Fig. 1. The heat flux at the gauge's hot active surface is computed in an inverse manner using temperatures measured at discrete locations along the gauge post [thermocouples (TCs) #1, 2, and 3, Fig. 1]. In

Received Sept. 19, 1996; revision received April 9, 1998; accepted for publication April 13, 1998.

*Mechanical Engineer, 9100 Keystone Crossing, Suite 200.
†Electrical Engineer, Sensors and Electronics Technology Branch, Instrumentation and Controls Division, 21000 Brookpark Road.
‡Retired, 21000 Brookpark Road.

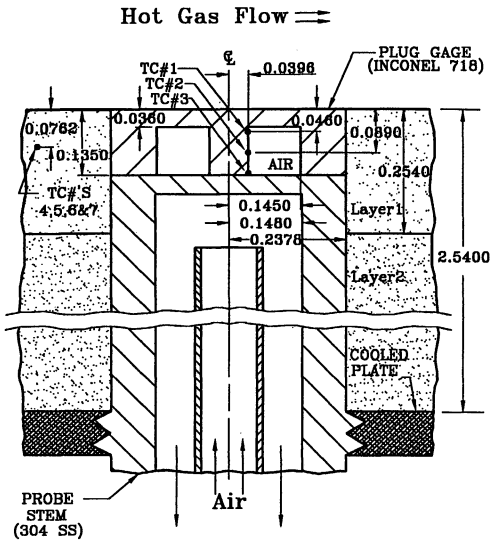

Fig. 1 Cross-sectional view of the gauge/probe assembly as mounted in the experiment. (All dimensions in centimeters.)

previous analyses the gauge post temperatures were used to develop an approximate axial temperature profile that was extrapolated to the hot active surface.[2-4] The approximate temperature profile is used to compute the surface axial temperature gradient and gauge heat flux. The extrapolation requires the assumption of one-dimensional heat flow between the gauge's hot active surface and the temperature measurement locations. Although favorable agreement between the measured heat fluxes of plug-type gauges and other gauge types has been shown, observation of the plug-type gauge geometry shown in Fig. 1 indicates that two-dimensional heat flow effects may not be insignificant. For example, the annular air gap within the gauge, which is necessary for placement of thermocouples within the gauge, will prevent the heat flow at the hot active surface from being purely one-dimensional. This and any other aspect of the gauge design or application that causes the heat flow through the gauge to not be one-dimensional may cause the heat flux indicated by the gauge to be different from the desired actual heat flux at the surface of the material that the gauge is mounted in.

It is the goal of this study to quantify two-dimensional effects and to assess related controlling factors in plug-type heat flux gauges. Experimental determination of two-dimensional effects is made difficult by the small geometry involved. Thus, a numerical analysis of a plug-type gauge is needed. Such an analysis was not found in the literature. While the numerical method used here is the alternating direction implicit (ADI) technique that is based on a transient model, and while some transient data are presented, the focus of the present study is on steady-state behavior. Analysis of plug gauge transient thermal behavior is left for future work.

Gauge and Experiment Description

Various plug-type gauges have been designed, built, and tested. The particular gauge analyzed in the present study was attached to an air-cooled probe, and tested in the 2 × 9 Turbulent Flow Duct Facility at NASA Ames Research Center. Details of the test facility are provided in Balter-Peterson et al.[5] The 2 × 9 Turbulent Flow Duct Facility utilizes a plasma arcjet heater upstream of a DeLaval nozzle to obtain a high-enthalpy supersonic flow in the test section. The test section is rectangular with a 5.1 × 23 cm (2 × 9 in.) flow cross section, with a design Mach number of 3.5.

In the test setup, the gauge probe assembly was mounted in one of the 23-cm (9-in.) walls, such that the metal gauge probe surface was flush with the internal test section surface. Figure 1 depicts the gauge and probe assembly mounted in the test-section wall. The wall in which the probe assembly was mounted consisted of two layers of rigid, poorly conducting material affixed to a cooled metal plate. Effectively, the wall consisted of two dissimilar layers of material labeled "Layer 1" (TUFI) and "Layer 2" (FRCI) mounted to a cooled metal plate as shown in Fig. 1. The other surfaces in the test section consisted of water-cooled metal plates.

The plug gauge body was constructed from Inconel alloy 718 and was laser/spot welded to the probe stem that was constructed from type S 304 stainless steel. Temperatures were measured in the gauge along the post at three locations, labeled "TC# 1," "TC# 2," and "TC# 3" in Fig. 1. The thermocouples were constructed from 0.0038 cm (0.0015 in.) diameter type K thermoelement wire and were tack welded to the post. The thermocouples were not aligned above each other as shown in Fig. 1, but were spaced around the cylindrically shaped post at 120-deg angles from each other.

Temperatures were also measured in the surrounding wall material during the experiment using four 0.025 cm (0.01 in.) diameter type K thermocouples. These thermocouples were located at a depth of 0.03 in. (0.076 cm) from the exposed wall surface. This approximate depth of the four thermocouples is shown in Fig. 1 (TCs #4, 5, 6, and 7), although in the actual installation the thermocouples were located at a radius of approximately 5 cm (2 in.) at various angular positions around the gauge.

Several test runs were made with the gauge in NASA Ames Research Center's 2 × 9 facility. The particular test chosen here for comparison with the numerical model is referred to as the "air-cooled probe" test. In this test air was steadily forced into the probe coolant channel to actively cool the gauge backface to maintain acceptable gauge hot surface temperatures. The gauge heat flux measurements were compared with those of several water-cooled reference calorimeters mounted across from the probe on the opposite wall of the test section. Despite the fact that the reference gauges were mounted in a water-cooled metal wall that had a significantly different surface temperature than the insulated wall in which the gauge probe assembly was mounted, agreement between the plug-type gauge heat flux measurements and the reference calorimeter heat flux measurements were within ±10%. Details of the comparison with the reference calorimeters can be found in Liebert and Kolodziej.[4]

Because the primary purpose of the test facility is for demonstrating material (and gauge) survivability, some information needed for modeling in the current study was not available and had to be approximated. Data collected during the experiment include static pressures, temperatures in the insulation, heater arc current and manifold pressures, and heat flux measurements taken from the reference calorimeters and plug-type gauges. The wall material in the experiment has low thermal conductivity and the effects of differing gauge and wall materials is investigated as part of this study. However, this gauge type is not limited to applications involving poorly conducting materials.[2,3]

Mathematical Model and Approximation of Physical Variables

The model domain consists of the gauge, the probe stem on which the gauge was mounted, and a portion of the surrounding material that the gauge and probe stem assembly was mounted in. All materials are modeled as being isotropic with temperature-dependent thermal properties. The form of the governing heat conduction equation that applies here is

$$\frac{1}{r}\frac{\partial}{\partial r}\left(rk_i\frac{\partial T_i}{\partial r}\right)+\frac{\partial}{\partial x}\left(k_i\frac{\partial T_i}{\partial x}\right)=\rho_i c_{pi}\frac{\partial T_i}{\partial t} \tag{1}$$

where i is an index corresponding to the different materials within the domain (Inconel, air, type S 304 stainless steel, and

wall materials). Curve fits of thermal conductivity and specific heat vs temperature are used for each of these materials. Property data sources include the Aerospace Structural Metals Handbook,[6] Touloukian and Ho,[7] and Incropera and DeWitt.[8] The curve fits approximate the tabulated property data to better than ±6% over the temperature range encountered in the calculations, with the exception of the gauge specific heat, which is within ±10% of the available data.

The gauge and wall surfaces exposed to the hot-gas flow are modeled as convecting and radiating, with the hot gas radiatively nonparticipating and the test section walls forming a radiatively gray enclosure at an approximated temperature of 339 K. The surface emissivities used for the gauge and wall are 0.88 and 0.85, respectively. The convective coefficients corresponding to the hot-gas flow over the gauge and wall will vary with position and time during a given test. Uniform (but different) convective coefficients are assumed for these two surfaces and are obtained as follows. The steady-state heat flux measured with the gauge was used to estimate the convective coefficient at the gauge's hot surface. For the surface of the wall that the gauge was mounted in, it is assumed that 99% of the incident convective heat transfer was reradiated to the surrounding test section walls. The hot-gas stagnation conditions and, hence, the recovery temperature are not known and had to be estimated. The recovery temperature was computed using an estimated flat-plate turbulent flow recovery factor, a Mach number assumed equal to the facility's design value, and a freestream static temperature that was estimated to be slightly above the measured steady-state temperature near the insulation surface, approximately 1900 K (2960°F). In the experiment, the hot-gas flow conditions were essentially ramped to steady-state values starting at time zero. The hot-gas recovery temperature is assumed to have varied in time in proportion to a weighted average of the measured upstream manifold pressure and arc current.

The annular volume of air within the gauge body is modeled as participating by pure conduction only. This is assumed to be a reasonable approximation because of the extremely small dimensions of the annulus.

The thermal contact resistances at the interfaces between the gauge body and probe stem and between the dissimilar wall layer materials are assumed to be negligible. The thermal contact resistance that existed at the interface of the gauge/probe assembly metal and the wall layers was not known and had to be estimated. This is a difficult parameter to estimate and its value most likely changed during the experiment because of hot gas permeating the interface gap and the different coefficients of thermal expansion of the materials involved. A constant and uniform value of thermal contact resistance at this interface corresponding to a 0.00254 cm (0.001 in.) thick layer of air at standard atmospheric pressure and 500 K (440°F) is used as a reference value.

The probe stem is assumed to be cooled by air at a constant temperature of 286.5 K (56.0°F). Separate but constant convective coefficients are utilized for the two air-cooled probe stem surfaces. Cooling of the probe stem base adjacent to the gauge occurs by jet impingement convection. The convective coefficient associated with one jet in an array of circular jets is used as a reference value for this surface.[9] Cooling of the outer periphery of the probe stem's coolant return channel occurs by annular flow. The convective coefficient associated with the outer surface of a fully developed annular flow is used as a reference value.[8] These two internal convective coefficients have to be computed using an estimate for the coolant mass flow rate, which was not measured during the experiment.

The lower boundaries of the probe stem and wall (cold plate boundary) are assumed to be held at a constant temperature of T = 286.5 K (56.0°F). The outer periphery of the model domain is modeled as being adiabatic. Several runs with different values of the model domain outer radius were made to assure that the computed results were independent of this radius. It was found that the necessary outer radius was four times that of the gauge radius when the gauge is mounted in the previously described poorly conducting wall material, and 11 times that of the gauge radius when the gauge is mounted in a like material (Inconel).

Numerical Model Description

The model is a two-dimensional, axisymmetric, time-dependent, finite difference model. The numerical solution of the discretized equations is performed using the ADI solution procedure.[10] This procedure is second-order accurate in space and time, i.e., $\mathcal{O}(\Delta x^2, \Delta r^2, \Delta t^2)$. In the ADI method the domain is swept first in columns, and the energy balance equations for all nodes in a given column are integrated from time level n to time level $n + 1/2$. The domain is then swept in rows, and the energy balance equations for all nodes in a given row are integrated from time level $n + 1/2$ to time level $n + 1$. Because of space requirements and the common use of this solution procedure for time-dependent two-dimensional conduction problems, derivation of the computational equations has been omitted and only the nodal equations for an interior node are given. Nodal equations for nodes along the domain boundary and along material interfaces will differ from the equations shown next. The equations used at all interior nodes were as follows.

Axial (x-direction) sweep:

$$B_x \times T_{i-1,j}^{n+1/2} + D_x \times T_{i,j}^{n+1/2} + A_x \times T_{i+1,j}^{n+1/2} = C_x \qquad (2)$$

Radial (r-direction) sweep:

$$B_r \times T_{i,j-1}^{n+1} + D_r \times T_{i,j}^{n+1} + A_r \times T_{i,j+1}^{n+1} = C_r \qquad (3)$$

where the coefficients B_x, etc. (for interior nodes only) are defined in the Nomenclature. The resulting system of equations for each row or column in the model domain are tridiagonal and are solved with the tridiagonal matrix algorithm given in Anderson et al.[10]

Various heat flux definitions are utilized in the present study. The local heat flux at the centerline of the gauge hot active surface is computed using the following energy balance on the centerline node of the hot active surface:

$$q''_{\text{surf,CL}} = (q_{\text{sto}} - q_p - q_b)/A_{\text{surf,CL}} \qquad (4)$$

where q_{sto}, q_p, and q_b are the heat storage, heat conducted from the periphery, and heat conducted from the bottom of the cell, respectively, and $A_{\text{surf,CL}}$ is the corresponding surface area of the cell.

The average heat flux over a larger portion of the hot active surface than that of the centerline cell is also of interest. The heat flux at the hot active surface, averaged over the post radius is defined as

$$q''_{\text{surf},p} = \frac{1}{A_{\text{post}}} \sum_{j=1}^{np} q_{\text{surf},j} \qquad (5)$$

where j represents the radial node index, np corresponds to the post radius, and A_{post} represents the surface area equivalent in size to the cross-sectional area of the post. Similarly, the average heat flux over the entire gauge hot active surface is defined as

$$q''_{\text{surf},g} = \frac{1}{A_{\text{gauge}}} \sum_{j=1}^{ng} q_{\text{surf},j} \qquad (6)$$

where ng corresponds to the gauge radius, and A_{gauge} represents the entire hot active surface area of the gauge.

The average axial heat flux in the gauge post at a given thermocouple location is defined as

$$q''_{post} = \left(-\int kr \frac{\partial T}{\partial x} dr\right) \Big/ \int r\, dr \qquad (7)$$

where the integrals are taken over the post radius. The temperature gradient in Eq. (7) is computed by using the predicted temperatures at the two grid points (axially) closest to the known axial position of thermocouple no. 1, 2, or 3 for each radial increment.

Because of the significant difference in length scales in the axial and radial directions, a variable grid spacing is used in the x direction. Specifically, an evenly spaced x-direction grid is used between the hot surface and a position just below the interface of wall layers 1 and 2. A linearly varying x-direction grid spacing, following Thompson,[11] is used throughout the remainder of the x domain. The radial grid spacing is uniform throughout the model domain. The model preprocessor can easily accommodate other axial grid spacing strategies, but none were investigated in the present study.

Except where noted, 83 axial nodes were used in the uniform grid-spacing region, spanning approximately 0.30 cm (0.12 in.), and 50 axial nodes were used in the variable grid-spacing region, spanning the remaining 2.24 cm (0.88 in.) of the x domain. The uniform grid cell sizes were chosen so that the gauge's post radius and the gauge's front wall thickness would both be fit with an integer number of cells. For the grid spacing described earlier the post radius was filled with 10 cells and the gauge (front) wall thickness was filled with nine cells. This resulted in a radial space step of 4.11×10^{-5} m (1.62×10^{-3} in.) and an axial space step in the uniform grid spacing region of 3.60×10^{-5} m (1.42×10^{-3} in.).

Model Verification

The geometry and physics of the problem in its complete form precludes verification with an exact solution. However, steady-state heat balances and simplified versions of the program were used to establish confidence in the model. Global energy balances around the model domain for steady-state conditions were satisfied to better than 0.1%.

A simplified version of the model was used to simulate a right circular cylinder with constant and uniform thermal properties, an adiabatic outer periphery surface, a convective top surface, and a constant temperature back face. In this manner, essential aspects of the original model were retained with the exception of the convectively cooled surfaces, temperature-dependent thermal properties, and hot surface radiation effects.

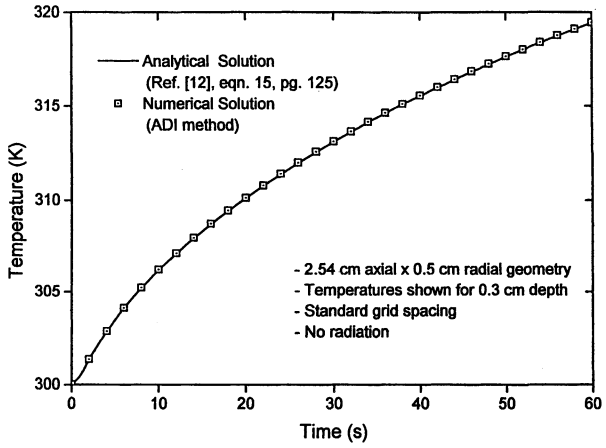

Fig. 2 Comparison of model results and analytical solution. Cylinder with adiabatic periphery, initially at 300 K with base held fixed at 300 K, with a step change in fluid temperature above top surface to 500 K. h = 100 W/m² K, α = 3.108E-06 m²/s, and k = 11.685 W/m K.

The model output generated by a step change in hot-gas temperature at the convective top surface was compared with exact solution results [Carslaw and Jaeger,[12] Eq. (15), p. 125]. Results are shown in Fig. 2, indicating excellent agreement.

Results and Discussion

A base case was run using the reference values described in the mathematical modeling section as model inputs. The specific parameter values were h_g = 479.2 W/m² K, h_w = 548.8 W/m² K, ε_g = 0.88, ε_w = 0.85, h_{jet} = 3824 W/m² K, h_{ann} = 1790 W/m² K, and $R''_{t,c} = 6.4 \times 10^{-4}$ m² K/W. For this base case, the measured steady-state temperatures at the post positions corresponding to TCs #1, 2, and 3 were all overpredicted by over 150 K. The predicted steady-state heat flux at the surface of the gauge, quantified by $q''_{surf,CL}$, was within 20% of the measured heat flux value. The steady-state temperature gradient in the gauge post, and the heat flux through the post as quantified by $q''_{post,TC1}$ was overpredicted by a factor of approximately 3.5. The measured steady-state temperatures in the insulation corresponding to TCs #4–7 were well predicted. The fact that the predicted post temperatures and temperature gradient, i.e., heat flux, did not agree with the measured steady-state temperatures was not surprising because several key factors of the experiment are not known and were estimated, namely the hot-gas flow conditions, the coolant gas flow conditions, and the interface thermal resistance between the gauge/probe assembly and the wall material. Because the temperature difference between the hot gas and the gauge surface is large in the experiment, it is not surprising that the overprediction in gauge temperature caused only a small underprediction of the surface heat flux. The overprediction of heat flux through the gauge post can be understood from the results presented later. Aspects of the model were investigated to ensure that calculations were being performed properly. Mesh refinement was performed by doubling the number of nodes in both dimensions. The computed hot surface centerline temperature was within approximately 2 K, $q''_{surf,CL}$ was within approximately 0.5%, and $q''_{post,TC1}$ was within approximately 2% of the respective values obtained using the standard mesh. Forcing the time step to be an order of magnitude smaller caused less than a 1% change in the computed heat fluxes and less than a tenth of a degree change in the computed hot surface centerline temperatures.

To obtain better agreement with the measured post temperatures and heat flux values, the hot-gas convective coefficient above the gauge, the probe stem convective coefficients, and the interface thermal resistance values used in the base case were adjusted. Good agreement with the measured temperatures and the temperature gradient in the post could not be obtained through adjustment of just one or two of these input parameters. Specifically, the changes were made by increasing the interface thermal resistance value, and decreasing the gauge hot surface and probe stem convection coefficient values. The change in interface thermal resistance had the primary effect of decreasing the predicted temperatures in the post, whereas the change in the convection coefficients significantly decreased the predicted temperature magnitudes and the predicted temperature gradients in the post. The specific values of the input variables used were h_g = 50 W/m² K, h_w = 549 W/m² K, h_{jet} = 2103 W/m² K, h_{ann} = 985 W/m² K, and $R''_{t,c}$ = 1.04E−03 m² K/W. Additionally, the Mach number was decreased to 2.

After making the previously described adjustments, excellent agreement with the experimentally measured temperatures was obtained, as shown in Figs. 3 and 4. Again, the emphasis here is on steady-state results. It must be noted that the hot-gas convective coefficients above the gauge and wall were varied in proportion to the arc current and manifold pressure over the first 25 s and held fixed at the preceding values after 25 s. This improved agreement over the transient portion of the test and better represented the dependency of these varia-

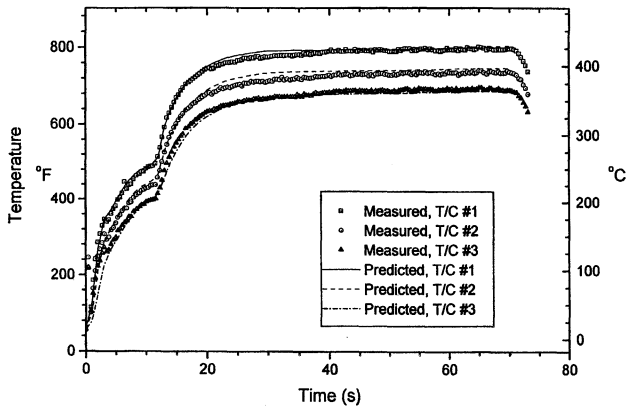

Fig. 3 Predicted vs measured post temperatures. Steady-state parameter values: h_g = 50 W/m² K, h_w = 549 W/m² K, h_{jet} = 2103 W/m² K, h_{ann} = 985 W/m² K, $R''_{t,c}$ = 1.04E−03 m² K/W.

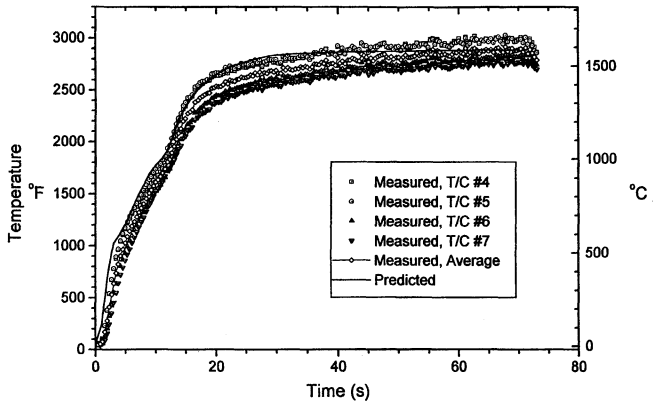

Fig. 4 Predicted vs measured wall temperatures. Steady-state parameter values: h_g = 50 W/m² K, h_w = 549 W/m² K, h_{jet} = 2103 W/m² K, h_{ann} = 985 W/m² K, $R''_{t,c}$ = 1.04E−03 m² K/W.

bles on the arc current and manifold pressure. Regardless of whether the variation of convective coefficients with time over the first 25 s is accurate, it should be noted that the same post and wall temperatures shown in Figs. 3 and 4 at time equals 70 s are predicted if the hot-gas convective coefficients are simply held fixed during the entire 0–70 s period. The hot-gas convective coefficients were forced to be constant at their steady-state values in all of the additional work reported next.

The predicted heat flux values for the case depicted in Figs. 3 and 4 are compared with the experimentally measured heat flux in Table 1. The values shown in Table 1 correspond to time equals 70 s, when approximately steady-state conditions prevail. It is observed from Table 1 that the heat flux predicted in the gauge post agrees well with the experimentally obtained heat flux value. However, the heat flux predicted at the gauge surface is significantly smaller than that predicted in the gauge post. It is also noted from Table 1 that the predicted heat flux at the gauge hot active surface is relatively uniform with respect to radius, a fact that is confirmed from a plot of surface heat flux vs radius for this case, discussed later.

To understand the good agreement depicted in Table 1 between the heat flux predicted in the gauge post ($q''_{post,TC1}$, and $q''_{post,TC2}$) and the measured heat flux, the method of computing the measured heat flux value must be understood. As explained earlier, the measured heat flux is computed from an estimate of the temperature gradient in the gauge at the hot surface. This estimated temperature gradient at the gauge hot surface is obtained by approximating the axial temperature profile between the gauge hot surface and the temperature measurement locations using an extrapolation of the temperatures measured along the gauge post. It turns out that the temperature distribution along the gauge post is relatively linear (see Fig. 3, near 70 s). Figure 3 attests to the fact that the temperature gradient in the post has been predicted accurately. Thus, the good agreement between the heat flux values predicted along the gauge post [$q''_{post,TC1}$, and $q''_{post,TC2}$ and the measured heat flux (Table 1)] is expected.

To understand the discrepancy between the heat flux predicted in the gauge post ($q''_{post,TC1}$ and $q''_{post,TC2}$) and that predicted at the gauge surface ($q''_{surf,CL}$, $q''_{surf,p}$, and $q''_{surf,g}$), consider the isotherm plot for this same case as shown in Fig. 5. Figure 5 shows the temperature distribution predicted in the gauge and nearby wall material at 70 s. From Fig. 5 it can be seen that the temperature distribution along the post is relatively linear, as claimed in the preceding text. However it is also seen that the predicted heat flow is not one-dimensional above the post; i.e., there is a radial component of heat flow in the vicinity of the gauge surface. Thus, it is seen that the two-dimensional nature of the heat flow under the hot active surface of the gauge is the reason for the difference in the predicted heat flux in the gauge post ($q''_{post\,TC1}$ and $q''_{post\,TC2}$) and at the gauge hot surface ($q''_{surf,CL}$). This is a significant observation, as the extrapolation method used in the measurement technique utilizes the assumption of one-dimensional (axial) heat flow between the temperature measurement locations and the gauge surface.

By observing the isotherms of Fig. 5, the cause of the two-dimensional heat flow can be determined. Specifically, it appears that some of the heat flowing through the gauge post originates from the gauge hot surface at radii greater than the post radius. This is logical because the air in the gauge cavity (assumed to have no bulk movement) has a thermal conductivity that is approximately three orders of magnitude smaller than the gauge metal. Thus, the annular air cavity around the gauge post acts to block axial heat flow, and some of the heat entering the gauge hot surface above the air cavity ultimately flows through the post. Again, it is pointed out that the air cavity is present to facilitate attachment of the thermocouples along the gauge post.

Table 1 Comparison of predicted and measured heat flux values for gauge mounted in poorly conducting material[a]

	Heat flux, MW/m²		Surface centerline temperature
Predicted	$q''_{surf,CL}$	0.105	
	$q''_{surf,p}$	0.105	
	$q''_{surf,g}$	0.103	713.2 K
	$q''_{post,TC1}$	1.11	
	$q''_{post,TC2}$	1.12	
Measured	1.1		725 K[b]

[a] Values obtained at 70 s. Same case as in Figs. 3–5.
[b] Approximated by extrapolation.

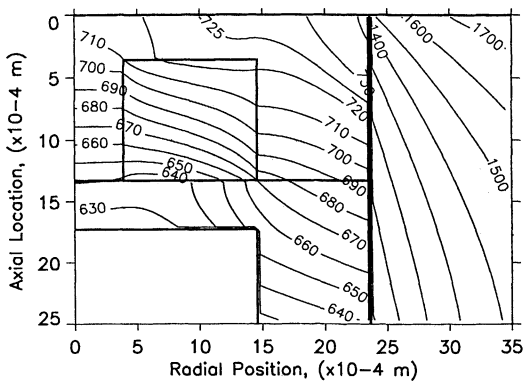

Fig. 5 Predicted temperature distribution at 70 s in the vicinity of the gauge post for gauge mounted in poorly conducting material (same case as shown in Figs. 3 and 4). A portion of the computational domain is not shown.

Table 2 Predicted surface centerline temperatures and heat flux values as a function of thermal resistance between gauge and wall[a]

$R''_{t,c}$, m² K/W	Surface centerline temperature, K	Heat flux, MW/m² $q''_{surf,CL}$	Heat flux, MW/m² $q''_{post,TC1}$
1.04×10^{-3}	713.2	0.105	1.11
1.04×10^{-2}	491.4	0.126	0.574
1.04×10^{-1}	386.1	0.133	0.376

[a]Values obtained at 70 s.

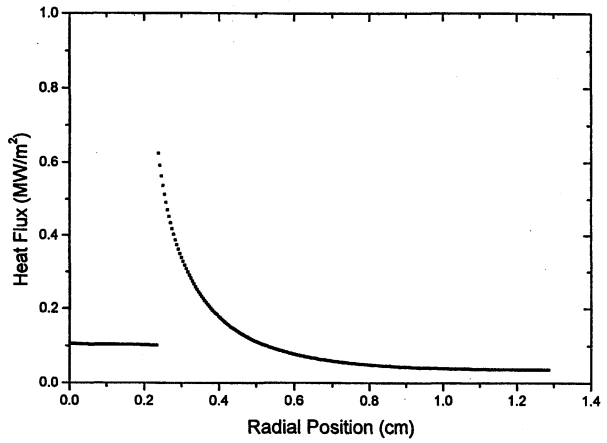

Fig. 6 Predicted surface heat flux distribution at 70 s for gauge mounted in poorly conducting material (same case as shown in Figs. 3–5).

As noted earlier the effect of the interface thermal resistance on the gauge is significant. Table 2 shows the effect of increasing the interface thermal resistance between the gauge and the wall. The increase in interface resistance dramatically controls the magnitude of temperatures within the gauge, but also notably affects the heat flow in the gauge. Specifically, as the interface thermal resistance is increased, the predicted gauge post and surface heat flux values come into closer agreement. This trend is logical because the effect of the reduced peripheral inflow of heat allows more of the heat entering the gauge hot active surface above the annulus of air to travel around the annulus's outer radius as it travels to the cooled channel below. However, while the trends seem logical and the results lend themselves to a better understanding of how heat transfer occurs in the gauge, it should be noted that the larger values of the interface thermal resistance values shown in Table 2 are unrealistic for the application being studied. The predictions do show how conditions at the gauge periphery influence gauge temperatures and heat flux.

The surface heat flux for the case depicted in Figs. 3–5 is shown in Fig. 6. Figure 6 illustrates that for this case the heat flux predicted at the gauge surface is not the same as the heat flux predicted along the surface of the wall in which the gauge is mounted. Specifically, the average heat flux over the gauge surface is predicted to be larger than the heat flux into the wall surface (at large radii, where the thermal field is not significantly affected by the presence of the gauge). This fact is not surprising because the surface temperature of the gauge is significantly lower than the surface temperature of the insulation, caused by the fact that the gauge is air cooled and the wall material has a significantly smaller conductivity than the gauge material. The large "spike" in the surface heat flux near the sensor periphery shown in Fig. 6 is because the convective coefficient used above the wall was larger than the convective coefficient used above the gauge, coupled with the transfer of heat from the hot wall surface to the relatively cold gauge outer periphery surface. This inwardly directed radial heat removal occurring under the hot wall surface causes the wall surface temperature near the gauge periphery to be lower than that at larger radii, which results in the surface heat flux into the wall decreasing with radius.

The preceding observations lead to the question of how the gauge behaves when mounted in a material that is more like the material that the gauge is constructed from. This question was examined numerically by studying the case of the gauge (constructed from Inconel) being mounted in Inconel. To model this situation the wall thermal properties of the previous cases were replaced with the gauge thermal properties, and the interface thermal resistance between the gauge and the wall is assumed to be negligible (a value of $R''_{t,c} = 6.4 \times 10^{-8}$ m² K/W was found to be sufficiently small). Additionally, the wall surface convective coefficient and surface emissivity (for the surface exposed to the hot-gas flow) were set to be equal to the corresponding values of the gauge hot surface. For this case, the original modeling variable values were used, specifically; $h_{hot\ surface} = 479.2$ W/m² K, $\varepsilon = 0.88$, $h_{jet} = 3824$ W/m² K, and $h_{ann} = 1790$ W/m² K.

The results for the case of the gauge mounted in Inconel are shown in Table 3. The results of Table 3 (see Standard gauge geometry) indicate that the surface temperature of the gauge is now hotter than that predicted in the previous cases (see the "Predicted" column, Table 1). This is because of the larger values of the convective coefficients used, and the better thermal contact between the gauge and the surrounding wall. The surface heat flux is also seen to be greater than the previous surface heat flux predictions. This also is primarily because of the larger value of the gauge hot surface convective coefficient being used in this case. However, the most notable information shown in Table 3 (gauge mounted in a like material) is that the predicted gauge hot surface heat flux and post heat flux values are now closer together compared with the results shown in Table 1 (gauge mounted in poorly conducting material). The fact that the predicted heat flux values at the gauge hot surface and the post in this case are closer together than in the case presented in Table 1 is consistent with the results obtained using a large (but unrealistic) interface thermal resistance between the gauge and the body (Table 2). Thus, mounting the gauge in a like material is seen to produce better agreement between post and gauge surface heat flux values than when the gauge is mounted in a dissimilar material.

A plot of surface heat flux for the case described in the preceding text (gauge mounted in a like material) is shown in Fig. 7. In this case the gauge experiences a small but noticeable variation in surface heat flux in the radial direction, which was not discernable in the previous case (Fig. 6). This variation is more noticeable in the present case because the average gauge surface temperature is closer to the hot-gas temperature and slight variations in surface temperature more strongly affect the quantity of local convective heat transfer. Radial variations in the surface heat flux just outside the gauge outer periphery are much smaller for the gauge mounted in a like material (Fig. 7) than for the gauge mounted in poorly conducting material (Fig. 6). This is not surprising because in the former case, there is no discontinuity in material properties and convective coefficients (and, hence, less variation in surface temperature) at the gauge periphery.

Table 3 Predicted heat flux values for gauge mounted in Inconel, steady-state results

Heat flux, MW/m²	Standard gauge geometry[a]	Gauge past radius doubled[b]
$q''_{surf,CL}$	0.799	0.833
$q''_{surf,p}$	0.796	0.826
$q''_{surf,g}$	0.796	0.807
$q''_{post,TC1}$	3.80	2.34
$q''_{post,TC2}$	3.82	2.35

[a]Centerline temperature, 1180 K.
[b]Centerline temperature, 1137 K.

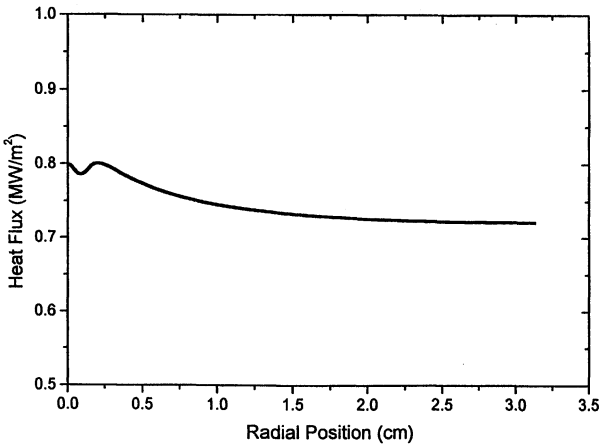

Fig. 7 Predicted steady-state surface heat flux for gauge mounted in like material (Inconel).

The results of Tables 1 and 3 ("Standard geometry") indicate that the differences between the gauge post and hot surface heat flux values are not just a result of the mounting and material property considerations; the differences are also related to the plug–gauge geometry as explained earlier. It is of interest to see how strongly the gauge geometry affects this difference. In general, to minimize the difference between the heat flux values at these two locations, one wants to minimize the difference between the hot surface area and the post cross-sectional area caused by the air gap. There are various ways to do this. In Table 3 results obtained using the actual gauge geometry are shown together with the results obtained with the post radius doubled (both for gauge mounted in Inconel with same geometry as seen in Fig. 1). It is seen that this increase in post diameter has a significant and favorable impact on the difference of the computed heat flux at the surface and in the post.

Artificially increasing the thermal conductivity of the air in the gauge and increasing the i.d. of the probe stem also improves agreement between the predicted gauge surface and post heat flux values. It should also be noted that an earlier version of the program, which utilized a constant and uniform heat flux boundary condition at the gauge hot surface, also showed differences between heat flux predicted in the gauge post and the heat flux at the gauge surface. The differences predicted were of the same general magnitudes as reported earlier using a convective boundary condition at the hot surface.

Summary and Conclusions

A two-dimensional, transient numerical finite difference model of a plug-type heat flux gauge/probe assembly, incorporating temperature-dependent thermal properties and surface radiation has been developed and demonstrated. The model predictions have been compared with experimental results. The model is shown to be capable of correctly predicting steady-state temperatures measured along the gauge post while simultaneously predicting a heat flux in the gauge post that is equal to the measured heat flux indicated by the gauge.

Until the present analysis the indicated heat flux of the gauge that was obtained by extrapolating the temperature profile in the gauge post to the hot active surface was assumed to be the same as the heat flux at the gauge's hot active surface. In the gauge post relatively linear axial temperature distributions with negligible radial gradients are observed experimentally (and are predicted by the model). However, measurements were not available to determine if two-dimensional heat transfer occurs in the region just under the hot active surface near the gauge's centerline. The numerical predictions presented in this study indicate that radial temperature gradients are significant in this important region of the gauge, at least for the cases studied. As a result, the quantity of heat flux at the hot active surface of the gauge is shown to be different from the heat flux in the gauge post, i.e., different from the heat flux indicated by the gauge. The magnitude of this difference is shown to be primarily because of the air gap geometry inherent in the gauge design, as well as to the thermal conditions at the outer periphery of the gauge.

Thus, the numerical model has been used to demonstrate that the two-dimensional heat flow is an important consideration in plug-type gauge design and measurement. The numerical model has been used to predict the heat flux entering the gauge's hot active surface using the measured temperatures within the gauge and to predict the heat flux entering the surface in which the gauge is mounted, at positions far enough away from the gauge as to be thermally undisturbed by the presence of the gauge. Experimentally, this means that the model can be used to determine heat flux into the undisturbed surface even when the gauge surface temperature is not the same as the undisturbed surface temperature.

From a design standpoint, two-dimensional effects can be reduced as the post radius is increased relative to the gauge body outer radius. The analogous situation of decreasing the gauge's internal annular air gap outer radius would also be beneficial. Backfilling the air gap with a thermally conducting but electrically nonconducting material, and minimizing the thickness of the gauge hot-surface wall are also recommended, although thermal stress considerations may limit the latter suggestion. Designing the probe stem coolant channel to have a larger i.d. than the gauge body would also be beneficial.

Advantages of the plug-type heat flux gauge include its nonintrusiveness and proven capability to withstand extremely harsh conditions. An examination of unpublished plug-type gauge data obtained using an arc lamp at NASA Lewis Research Center over the past 10 years support the preceding suggestions; these suggestions appear to be particularly beneficial at longer steady-state test times, i.e., several minutes, and at lower heat fluxes, i.e., 0.01 MW/m^2).

Acknowledgments

The work described was performed at NASA Lewis Research Center while the first author was on a NASA/ASEE Summer Faculty Fellowship. The support of NASA and the American Society of Engineering Education is gratefully acknowledged. The authors also wish to acknowledge Paul Kolodziej of NASA Ames Research Center for fruitful technical discussions related to the test simulation.

References

[1]Diller, T. E., "Advances in Heat Flux Measurements," *Advances in Heat Transfer*, edited by J. P. Hartnett, T. F. Irvine, and Y. I. Cho, Vol. 23, Academic, San Diego, CA, 1993, pp. 279–368.

[2]Liebert, C. H., "Miniature Convection Cooled Plug-Type Heat Flux Gauges," NASA TM106483, 1994.

[3]Liebert, C. H., "Miniature High Temperature Plug-Type Heat Flux Gauges," NASA TM105403, 1992.

[4]Liebert, C. H., and Kolodziej, P., "Dual Active Surface Heat Flux Gage Probe," NASA TM106861, 1995.

[5]Balter-Peterson, A., Nichols, F., Misfud, B., and Love, W., "Arc Jet Testing in NASA Ames Research Center Thermophysics Facilities," AIAA Paper 92-5041, Dec. 1992.

[6]*Aerospace Structural Metals Handbook*, Vol. 4, CINDAS/USAF CRDA Handbook Operations, Purdue Univ., West Lafayette, IN, 1991.

[7]Toloukian, Y. S., and Ho, C.Y., (eds.), *Thermophysical Properties of Matter*, Plenum, New York, 1972.

[8]Incropera, F. P., and DeWitt, D. P., *Introduction to Heat Transfer*, 2nd ed., Wiley, New York, 1990.

[9]Martin, H., *Advances in Heat Transfer*, edited by J. P. Hartnett and T. F. Irvine, Vol. 13, 1977, Academic, San Diego, CA, pp. 18–22.

[10]Anderson, D. A., Tannehill, J. C., and Pletcher, R. H., *Computational Fluid Mechanics and Heat Transfer*, Hemisphere, New York, 1984.

[11]Thompson, J. F., *Handbook of Numerical Heat Transfer*, edited by W. J. Minkowycz, E. M. Sparrow, G. E. Schneider, and R. H. Pletcher, Wiley, New York, 1988.

[12]Carslaw, H. S., and Jaeger, J. C., *Conduction of Heat in Solids*, 2nd ed., Oxford Univ. Press, Oxford, England, UK, 1959.